# Development of a Miniaturized and Monolithic Spatial Heterodyne Spectrometer (SHS) Breadboard for Atmospheric Oxygen Emission Measurement

**Michael Deiml [(1)], Hans Thiele [(1)], Lumir Osmančík[(2)], Pablo Rodriguez Robles[(1, Now 3)], Pavlína Provazníková[(2)]**

*[(1)] OHB System AG, Manfred-Fuchs-Straße 1, 82234 Weßling, Germany, +49 (0)8153 4002-0, info.oberpfaffenhofen@ohb.de*
*[(2)] Meopta - optika, s.r.o, Kabelíkova 1, 750 02 Přerov, Czech Republic, +42 (0)581 241 111, info@meopta.com*
*[(3)] Onera,* Châtillon, *France, 6 Chem. de la Vauve aux Granges, 91120 Palaiseau, France, +33 (0)180386060*

## Abstract

With the ongoing trend of spacecraft miniaturization in the Low Earth Orbit, optical instruments also need to become smaller while still achieving high performance. For spectral measurements, alternative types to the classically used spectrometers like grating spectrometers or Michelson interferometers may be advantageous if these spectrometers can achieve high sensitivity within a small volume. The Spatial Heterodyne Spectrometer (SHS) is such a type of instrument. It is a Fourier-transform spectrometer similar to a Michelson interferometer but with gratings instead of mirrors in its arms.

The MiniSPEC project developed a breadboard instrument based on a monolithic Spatial Heterodyne Spectrometer (SHS) within a TRP activity of ESA. The selected use-case for the spectrometer is the observation of the Oxygen A-band molecular emission band that can be used to derive temperatures in the middle atmosphere. The breadboard spectrometer was developed for the later use in a CubeSat or microsatellite. The focus of the development lay on the manufacturing, assembly, and alignment of the SHS to develop a well-controlled and stable process for small series production of these kinds of instruments.

Through this project, key technologies and methods have been developed that allow to specify such instruments based on mission parameters, to design for athermal and monolithic SHS that can be analysed with an extensive tool suite tailored for SHS optical systems. Thorough and tight interaction loops between design and manufacturing disciplines allowed designing for manufacturing, assembly, and alignment. The ultra-high precision manufacturing capabilities at MEOPTA facilitated the controlled and reproducible alignment of SHSs, rendering batch and small series production feasible. The SHS could be characterized at OHB using state of the art, calibrated, and highly precise metrology setups for spectral, radiometric, geometric calibration, and the correction of instrument artefacts.

The design specification of the instrument was achieved within the first iteration, demonstrating that the design, manufacturing, and assembly process were well understood and controlled to achieve the required tight tolerances. Thus, a miniaturised Spatial Heterodyne Spectrometer suitable for oxygen A-band emission detection could be developed. An extensive test campaign demonstrated further that the instrument theory is well understood through consistency between theory and practice in key instrument parameters.

# 1. INTRODUCTION

## 1.1. Spectrometers

Spectrometers build the underlying basis in many fields for spectral measurements and diagnostics. These types of systems are also regularly used in instruments of remote sensing satellites to detect fire, determine the status of crops, monitor relevant climate change contributors, or to estimate the composition of exo-planets to name some examples.

Grating spectrometers are quite commonly used in remote sensing instruments in the visible and near infrared wavelength region, especially when a large spectral range with moderate spectral resolution should be observed. Michelson interferometers are used especially in the infrared range, due to their inherent advantages in this region, but also in the visible range if very high spectral resolutions are required. This high resolution comes with the cost of a more complex system that has moving parts, making it more sensitive to vibrations and potentially requires considerably more volume. Fabry-Perot spectrometers may be a solution when only a narrow spectral bandwidth needs to be observed with high spectral resolution and high sensitivity. These spectrometers require most often moving parts for spectral tuning and a high surface planarity that can become challenging and costly to manufacture.

Static Fourier-transform spectrometers are another type of spectrometers that have benefits that are especially useful for certain remote sensing applications from satellites. The here discussed Spatial Heterodyne Spectrometer (SHS) is an imaging static Fourier-transform spectrometer that exhibits useful characteristics for applications where a high spectral resolution over a small bandwidth is sufficient and a ruggedized, insensitive design is of major importance.

The SHS was first postulated by Cones in 1958 [1]. But due to the limitations of detector technology at that time, its applicability was limited. Only in 1992, when Harlander started again with the research and development in this type of spectrometer, its usefulness became apparent. Since then, SHS for different applications have been built up in the laboratory [2], have been flown on a Space Shuttle mission [3], on stratospheric balloons [4], on ballistic rockets [5], and as instruments on satellites [6],[7].

The SHS can be built as a monolithic instrument that makes it rugged and less sensitive to vibrations, which is especially useful to survive the launch loads of a rocket. It has a higher light sensitivity compared to grating spectrometers or classical Michelson interferometers. Thus, it can be designed small enough to fit within a CubeSat or small satellite. By selection of appropriate materials, it can be designed athermal [8], which is also especially useful for CubeSats where usually little power is available for active temperature control.

These advantages come with a trade-off between bandwidth and resolving power for a given instrument size, which is inherent for this type of instrument. However, the application for which this particular SHS is designed for suites the characteristics of the SHS very well.

## 1.2. Application Scenario

The SHS is developed for the application of remote sensing through limb sounding for the measurement of oxygen A-band spectra to retrieve temperatures in the middle atmosphere. This information is useful to characterize gravity waves (also called buoyancy waves) that are an important transport mechanism of energy and momentum from the lower atmosphere up into the upper atmosphere. The key idea behind the measurement is to measure the relative intensity of a few rotational lines of the oxygen A-band structure to derive the temperature. Thereby, a relative calibration of the instrument is sufficient and a narrow bandpass is desired.

The atmosphere is opaque for the oxygen A-band emission down to approximately 60 km altitude. The oxygen A-band emission from the altitude range of 60 km to approximately 120 km can be detected by a space based limb sounding instrument. Thereby, different production mechanisms exist for the relevant excited oxygen emission state. During night-time, only the Barth process is active that limits the emission to the altitude range from approximately 85 km to 95 km.

Figure 1-1 illustrates this observation case. The instrument on the satellite views the limb tangentially to the surface of the Earth where the atmospheric emission layer is located. The field of view in horizontal direction extends at the limb over several kilometres. The vertical resolution of 1 km at 90 km altitude is relevant for the dimensioning of the instrument. It is illustrated with a coloured strip in Figure 1-1.

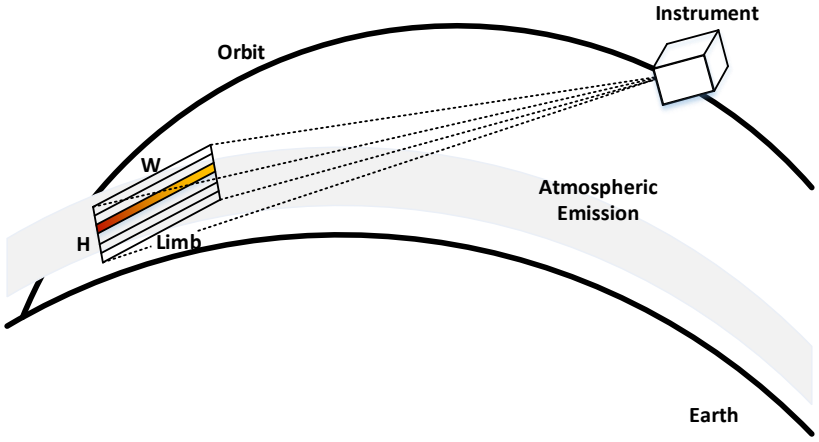


**Figure 1-1: Observation case for remote sensing instrument.**

## 2. THE SPATIAL HETERODYNE SPECTROMETER

### 2.1. Basic Principle

The SHS consists in its simplest realization of a beamsplitter and two reflection gratings, one in each arm. Consider a planar wavefront with a specific wavelength $\lambda_L$ perpendicular to the optical axis that reaches an ideal beamsplitter, where it is splitted. Both, the transmitted and the reflected wavefronts travel towards gratings which are tilted with a specific angle $\theta_L$, but in opposite directions in each arm. The rotation angles are such that planar wavefronts with the specific wavelength $\lambda_L$ are reflected back in exactly the same direction. This is achieved for the Littrow condition and thus, the wavelength $\lambda_L$ is the Littrow wavelength and $\theta_L$ the Littrow angle. Once the wavefronts constructively interfere, a constant intensity can be measured.

However, if the input wavefront has a wavelength $\lambda_L + \delta\lambda$ different than $\lambda_L$, the wavefronts get tilted when reflected back at the gratings. The tilts of the wavefronts depend thereby on the distance $\delta\lambda$ to the Littrow wavenumber $\lambda_L$ and the tilts have opposite signs in the two arms, because the gratings are tilted in the opposite directions. Once the wavefronts interfere again, the optical path difference, due to the tilts of the wavefronts, creates an interference pattern with constructive and destructive interference depending on the position on the detector (in the direction of the grating tilt). Thus, Fizeau fringes with a specific spatial frequency can be observed on the detector. The spatial frequency depends on the tilts of the wavefronts which in turn depend on the difference between wavelength and Littrow wavelength. This is the heterodyne aspect of the instrument. The response to non-monochromatic light is the summation of fringe patterns of different spatial frequencies. A Fourier-

transformation allows to retrieve the intensity in dependence of spatial frequency and if the Littrow wavenumber is known, also in dependence of wavelength: The spectrum.
The discussion shows that a few aspects are the defining properties of an SHS. The Littrow wavelength defines in which wavelength range the SHS can operate and defines the relation between spatial frequency and wavelength. Thus, it is important for precise spectral measurements to know the Littrow wavelength and to keep it stable during measurement. The spectral bandwidth is limited by the maximum resolvable spatial frequency, which depends on the sampling of the interferogram according to the Nyquist theorem. The SHS operates symmetrically around the Littrow wavelength that spectral signatures at wavelength $\delta\lambda$ cannot be distinguished from signatures at $-\delta\lambda$. Typically, a bandpass filter is employed that only light with wavelengths larger/smaller than the Littrow wavelength is detected.
The next important aspect is the resolving power of the SHS. Theoretically, the resolving power is the total number of illuminated grating grooves as it is for a conventional grating spectrometer. However, in practice the resolving power is lower, because apodization is required.
The visibility of an SHS, defined by $(I_{max} - I_{min})/(I_{max} + I_{min})$, is a performance metric that defines how much light contributes to useful and retrievable information. All energy that is not modulated does not provide information but contributes to an offset that increases the measurement noise and thus reduces the signal to noise ratio. The visibility varies with spatial frequency and typically decreases with increasing spatial frequency due to diffraction and optical aberrations.

### 2.2. Fore- and Detector Optics

The explanation of the SHS principle used a planar wavefront as output of an afocal telescope as fore-optics as example. Such a telescope as fore-optics is in general possible, but it provides distinct disadvantages compared to a focusing telescope, because a tilt mechanism is required to sample the atmosphere and the focal length needs to be fairly large for a limb sounding application.
The ideal solution is an anamorphic telescope that images the scene onto the gratings along the grating grooves and collimates perpendicular to the grating grooves. Thus, the vertical profile of the atmosphere can be sampled and horizontal features in the atmosphere are averaged out.
However, an anamorphic telescope is more complex in its components and is more challenging to build for high performance and a small volume. A compromise is to use the SHS with a focusing fore-optics. This means that the scene in the atmosphere is imaged onto the gratings of the SHS. Thereby, one spatial dimension, in this case the horizontal direction in the atmosphere, is overlaid with spectral information. The second spatial dimension, in this case the altitude/vertical direction, remains unchanged. This approach is acceptable, as the horizontal information content in the atmosphere is averaged out due to the long path length through the atmosphere, especially for high spatial fluctuations in the atmosphere that would coincide with spatial frequencies from the spectrum.
A detector optics behind the SHS has the task to image the gratings onto the detector. It allows by adjusting its magnification to fine tune or trade between spatial resolution and spatial bandwidth. Figure 2-1 shows a conceptual schematic of an SHS with a focusing fore-optics that has a bandpass filter in front, the SHS with its main components, beamsplitter, field-widening prisms, and gratings, and a detector optics. The function of the field-widening prism is the topic of the next section. The fore-optics images the scene onto the gratings which is then reimaged by the detector optics onto the detector.

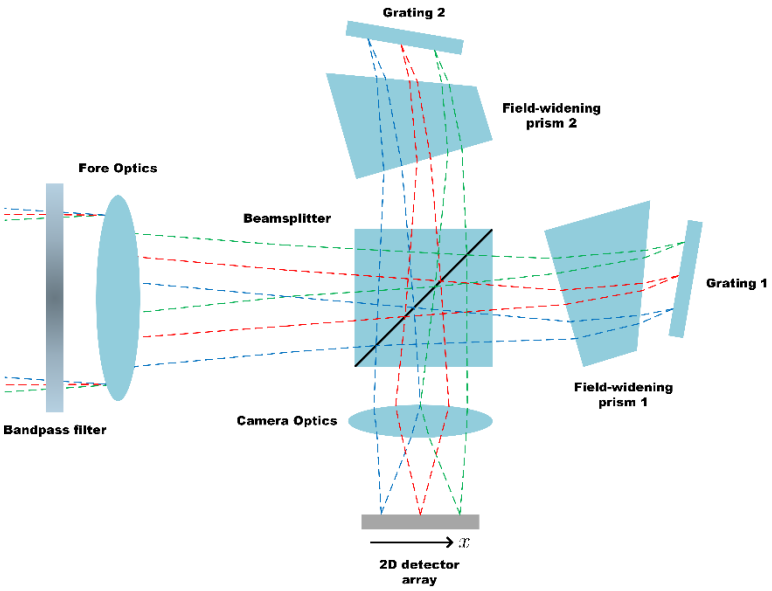


Figure 2-1: Conceptual schematic of an SHS instrument with focusing fore-optics.

## 2.3. Field-widened SHS

The basic SHS without field-widening prisms has only limited usefulness in practice, especially when it is used in a focused configuration. The introduction of field-widening prisms is therefore most often necessary. Field-widening prisms virtually rectify the gratings that they are perpendicular to the optical axis. This means for an SHS in a collimated configuration with a planar input wavefront that the influence on contrast of the wavefront incidence angle is considerably reduced, allowing for a larger NA of the instrument.

For an SHS in focused configuration, the field-widening prisms actually fulfil their name and increase the field of view of the instrument. Without field-widening prisms, the gratings would only be in focus at one field point, e.g. in the centre of the field, and will blur with increasing distance from this point. The larger spot sizes reduce the contrast of the interferograms. The rectification of the field-widening prisms reduces the dependence of the blur on image position and thus effectively increases the allowable field of view. Figure 2-2 illustrates this effect.

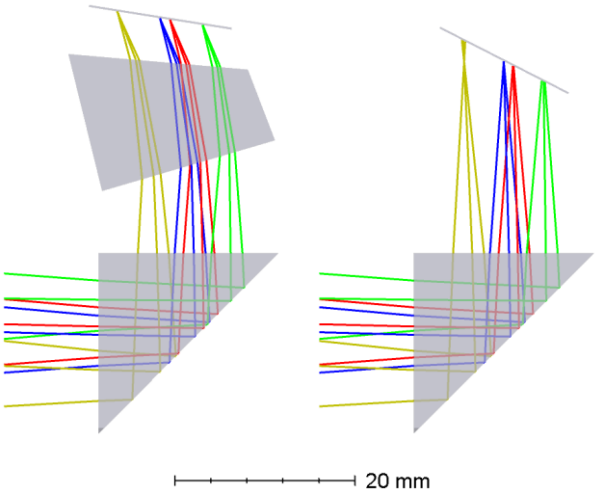


Figure 2-2: Illustration of field-widening effect of prisms for an SHS in focused configuration.

# 3. THE MINISPEC BREADBOARD

## 3.1. Design Parameters

The MiniSPEC breadboard is built as a laboratory demonstrator for a limb sounding application. Thus, the basic design parameters are derived from such an application. Table 3-1 summarizes the parameters. The fore-optics is defined by the limb observation altitude range that defines the vertical field of view and the horizontal field of view. Its focal length of 300 mm allows to image the scene onto a standard 2/3 inch (8.8 mm x 6.6 mm) image format with an instrument F-number of 5.6. It can then be reimaged by the detector optics with a 1:1 magnification onto a standard 2/3 inch detector. The Littrow wavenumber of 762 nm together with the bandpass Full-Width Half Maximum (FWHM) of 4 nm and a spectral resolution of at least 8000, define the spectral properties required to measure the oxygen A-band emission spectrum.
This particular selection of design parameters allows a flexible instrument setup that was the goal of this breadboard, because commercial fore- and detector optics can be tested that are adjustable in F-number.

**Table 3-1: Design parameters for the MiniSPEC breadboard**

| | |
|---|---|
| Limb Observation Altitude Range [km] | 68 - 112 |
| Vertical Spatial Resolution [km] | 1 |
| Horizontal Spatial Resolution [km] | 57 km |
| Resolving Power $\lambda/\Delta\lambda$ [-] | > 8000 |
| Instrument F-number [-] | 5.6 |
| Fore-Optics Focal Length [mm] | 300 |
| Littrow Wavelength [nm] | 762 |
| Bandpass FWHM [nm] | < 4 |

## 3.2. Design Drivers

Design drivers can be divided into drivers for the SHS and for the complete instrument. One general design driver for the SHS is the volume constraint together with the minimal required resolving power. For a larger resolving power, the SHS needs to increase in size as the grating groove density can only increase to a certain extent due to manufacturing technology and as the resolving power of the SHS is defined by the total number of grooves that are imaged.
Another design driver for the SHS is the required SNR that is limited by the maximum integration time, the size and the Numerical Aperture (NA) of the SHS. The etendué of the SHS influences the SNR. The etendué can be defined by the grating groove area times the NA at the grating. Considering that the SHS should be built fairly small to fit within a small satellite or CubeSat – while fulfilling the resolving power requirement – then the NA of the SHS can be used to increase the etendué. However, the larger the NA, the worse the performance of the SHS, because aberrations increase that reduce the visibility. Lower visibility means that the less light contributes to the modulated signal that is used for spectrum reconstruction (increasing the SNR), but more light contributes to a constant offset. The shot noise of the constant offset reduces then the SNR. Thus, at some point, increasing the NA of the instrument becomes detrimental to the SNR. Increasing the SNR is then only possible with the size of the SHS, which is constraint by the maximum envelope, or with the integration time which is limited by mission operations or scientific requirements.
The main design driver for the fore- and detector optics both are the volume constraint of the instrument. For a desired observation geometry that defines the focal length of the system and a desired SNR that defines the required aperture, the size of the fore-optics is almost defined.

Considering the application of remote sensing, the fore-optics is most likely a telephoto lens where its physical length is limited by the focal length and a typical telephoto ratio larger than 0.7.
For the detector optics, the volume constraint is also a major design driver, but the reason is different than for the fore-optics. The ideal detector optics is an object- and image-side telecentric lens with a large object-side NA. However, these lenses tend to become large and a suitable packaging needs to be found to accommodate such a lens within the available volume.

## 3.3. Optical Design

### 3.3.1. SHS Design

This section describes the baseline design. The Littrow wavelength is 762 nm. A grating groove density of 1200 lines/mm is selected as this is a commonly used value for grating manufacturers and it fits well to the resolving power requirement with considerable margin. The theoretical resolving power of the instrument is 20268. The minimum and maximum wavenumbers of the instrument are defined by the filter bandwidth less than 4 nm. The number of vertical samples stems from the altitude resolution requirements with considering the observation geometry. The number of spectral samples is determined by the detector to 2448 samples. These samples may be binned to together to increase the SNR ratio while the maximum spatial frequency within the filter bandwidth is still oversampled. For the maximum filter bandwidth, the maximum spatial frequency calculates to 142.4 lines/cm as worst case. The SHS design parameters are summarized in Table 3-2.

**Table 3-2: SHS Design Parameters**

| | |
|---|---|
| Littrow Wavelength [nm] | 762 |
| Grating Groove Density [lines/mm] | 1200 |
| Diffraction Order [-] | 1 |
| SHS Virtual Image Size horizontal/spectral [mm] | 8.4 |
| SHS Virtual Image Size vertical [mm] | 6.6 |
| Number Samples Vertical | 45 |
| Number Samples Horizontal/Spectral | 2448 |
| Littrow Angle [deg] | 27.21 |
| Theoretical Resolving Power @ Littrow Wavelength [-] | 20268 |
| Spectral Resolution @ Littrow Wavelength [pm] | 38 |

An image of the Zemax model of the SHS is shown in Figure 3-1. The fore-optics is simulated with an ideal paraxial lens with 300 mm focal length and an F/#=5.6. The SHS consists of a beamsplitter, two field-widening prisms, and two gratings. Figure 3-2 shows only one arm of the SHS, that the position of the virtual image plane becomes visible. The image plane is imaged by the detector optics onto the detector. The optical model represents a fully optimized SHS in this configuration and with the selected materials.

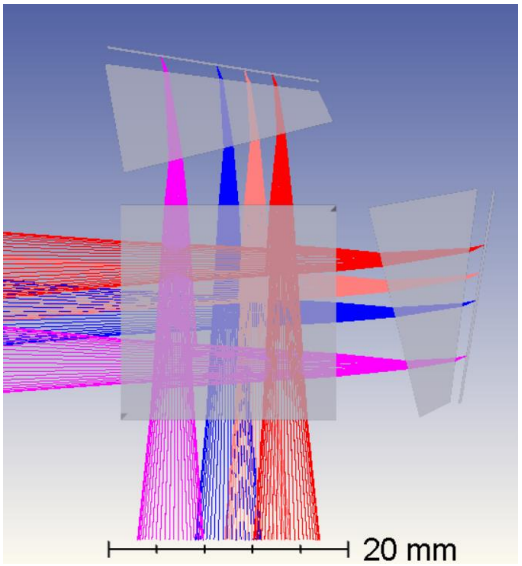


Figure 3-1: Design of the SHS

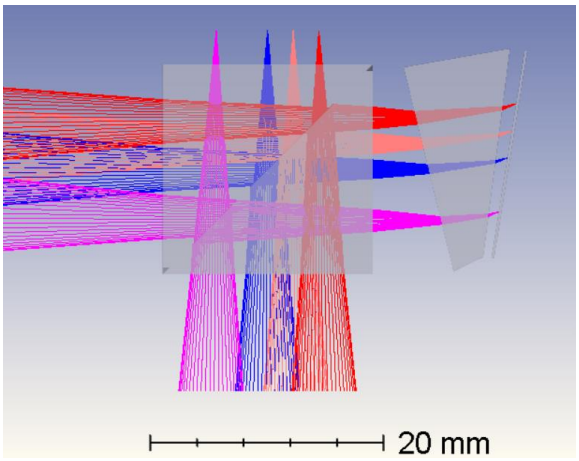


Figure 3-2: Design of the SHS with only one arm and visible virtual image plane

### 3.3.2. SHS Performance

The optical analysis is performed based on the Zemax model of the SHS with an ideal paraxial fore-optics lens. The optical performance is evaluated at the virtual image plane of the SHS. The virtual image plane is the position of the grating image if looking from the exit into the SHS. It differs from the real grating position due to the field-widening prisms. The optical performance analysis for the SHS in a focused setup is more involved compared to the afocal setup, because the individual PSFs of both arms need to be coherently added for many field points and then distributed over the image plane. Afterwards, the PSFs are interpolated over the complete image to calculate the interferogram. The outcome of the calculation is the interferogram for a specific wavenumber. The analysis considers optical aberrations, geometric distortions, and polarization effects. Figure 3-3 and Figure 3-4 show two exemplary interferograms and a cut through the vertical centre of the image. The difference between the two interferograms is that the wavenumbers were chosen such that the spatial frequencies are 5 and 105 fringes over the detector width, respectively. In both interferograms, the overlaying envelope caused by the optical performance of the system can be seen in the decrease of peak intensity and increase of bottom intensity towards the edges of the images.

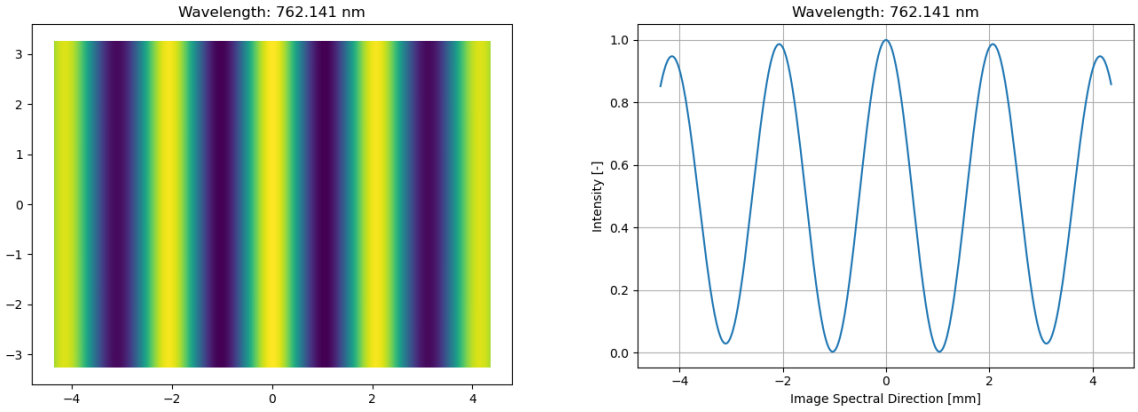


Figure 3-3: Right: Interferogram for wavenumber 13120.93 $cm^{-1}$. Left: Cut at vertical centre through the interferogram

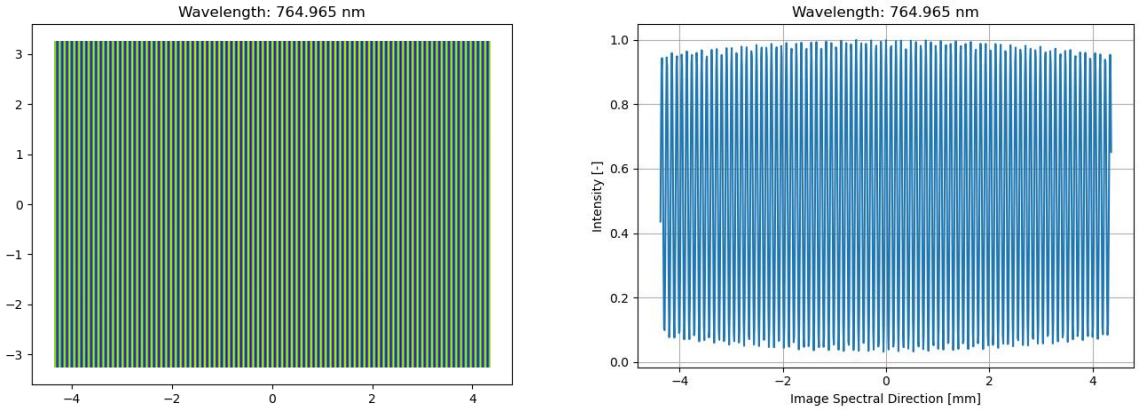


**Figure 3-4: Right: Interferogram for wavenumber 13072.49 cm$^{-1}$. Left: Cut at vertical centre through the interferogram**

These two interferograms together with many others can be used to calculate the resolving power and the visibility in dependence of spatial frequency. The result for the visibility analysis is shown in Figure 3-5. The mean visibility is between 80% and 90% for the complete spatial frequency range and decreases with higher spatial frequency. The visibility for zero spatial frequency is about 10%, which would be ideally 0% (flat image), and corresponds to the lower optical performance towards the edges of the field. Similarly, the standard deviation in the visibility is about 20%, because the visibility value is the mean visibility over all fringes in the interferogram. As the performance degrades towards the edges of the images, the visibility also degrades and increases the standard deviation over all fringes.

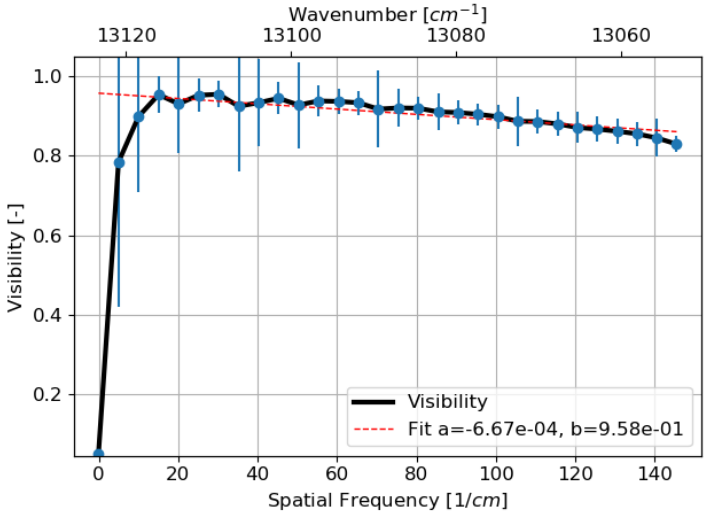


**Figure 3-5: Visibility vs. spatial frequency for the simulated interferograms.**

The analysis of the resolving power is more complex regarding the data processing of the interferograms. First, the interferograms are flattened, apodised, zero-padded, and then transformed into Fourier-space to fit the peaks of the spectrum with a 2D Gaussian distribution. The standard deviation of the Gaussian distribution is converted into FWHM, which is used as wavelength difference ($\Delta\lambda$) in the definition of the resolving power ($\lambda/\Delta\lambda$).

Figure 3-6 and Figure 3-7 show the resolving power in dependence of spatial frequency with the difference that the apodization is switched off for one image. For apodization, a 2D-Hanning function is used as a good compromise between loss in resolving power and side-lobe suppression. The resolving power without apodization is about 19500 (compared to the 20268 theoretical value) and

about 12100 with apodization. Thus, apodization with Hanning reduces the resolving power by about 0.63.

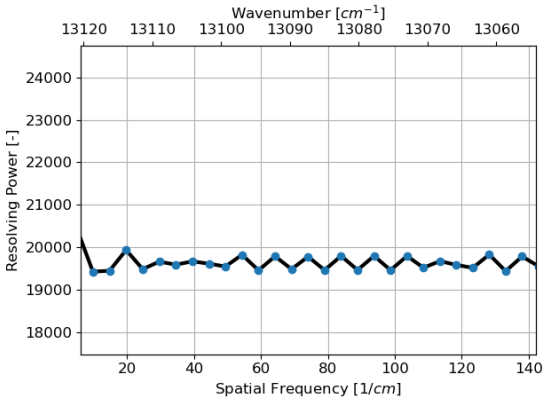


**Figure 3-6: Resolving power vs. spatial frequency for spectra without apodization (Hanning).**

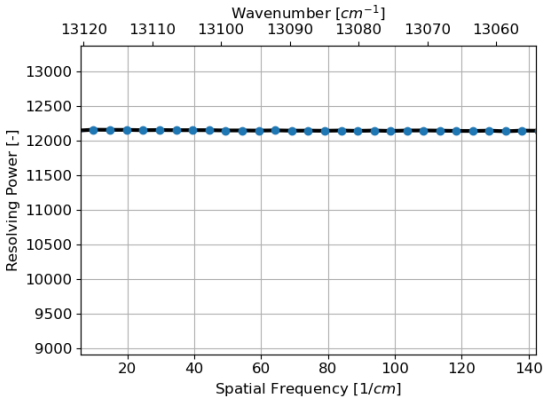


**Figure 3-7: Resolving power vs. spatial frequency for spectra with apodization (Hanning).**

### 3.3.3. SHS Materials

The design and performance evaluation implicitly assumed already some materials. The selection of the materials is based upon three main aspects. The glasses N-SF57 for the field-widening prisms and N-BK7 for all other components are a good compromise between the aspects performance, temperature stability, and mechanical stability.

1) **Performance**: The higher the refractive index of the field-widening prisms, the higher the performance, because the wedge angles of the field-widening prisms become smaller, reducing aberrations.
2) **Temperature stability**: In [8], the temperature stability of SHS regarding the stability of the Littrow wavenumber temperature gradient was analysed in depth. The lower the Littrow wavenumber temperature gradient, the higher the operational temperature range of the spectrometer, because if the Littrow wavenumber moves closer to the relevant spectral lines, light at the other side of the Littrow wavenumber will interfere with the relevant spectral lines. If the Littrow wavenumber moves further away from the relevant spectral lines, spatial frequencies will increase and aliasing occurs which reduces measurement precision. The analysis approach used in [8] was also used in this project to analyse temperature stability of the SHS to -0.0780 $cm^{-1}$/°C.
3) **Mechanical stability**: The field-widening prisms and the gratings need to have different glasses for temperature stabilization, but depending on the glasses, the CTE mismatch may lead to a lower operational temperature range due to structural integrity.

### 3.3.4. Fore- and Detector Optics

Commercial lenses have been selected for the MiniSPEC breadboard to focus the development towards the SHS as its core.

The fore-optics lens NIKON AF-S NIKKOR 300mm 1:4E PF ED VR is a state-of-the-art consumer lens with a theoretical MTF of 50 lines/mm at 50% contrast for an F-number of 5.6. The particular sourced lens has a MTF50 value about 40 lines/mm by measurement.

The lens Lensagon TC10M-10-65I is a high resolution telecentric lens designed for a resolution (object side) of 3.05 µm for an object size of 8.8 mm x 6.6 mm. Its numerical aperture with 0.11 is

sufficiently large enough (0.11 > 0.09 (F/#=5.6)). Its distortion is very low with only 0.03% and the lens has theoretically nearly diffraction limited performance at 762 nm (> 100 lines/mm @ 50% contrast). The MTF measurement shows that the MTF for the particular lens has an MTF50 value of 80 lines/mm.

### 3.4. Mechanical Design

The mechanics of the MiniSPEC breadboard is designed for flexibility with many possible alignment degrees of freedom. The SHS is first mounted onto a stainless steel plate with similar CTE as the glass components. It is in turn mounted into the light-tight aluminium housing.
The detector is mounted onto the detector-optics by a C-mount interface. These two components are then mounted with a custom interface onto the SHS housing. Alignment of five degrees of freedom enables to experiment and optimize for best optical performance. The fore-optics is mounted with a standard Nikon F-mount onto the SHS housing. This interface has four degrees of freedom.
Figure 3-8 shows the instrument breadboard including the commercial fore-optics, detector optics, and detector. Figure 3-9 shows the manufactured and assembled SHS housing with its interfaces.

**Figure 3-8: Mechanical design of the SHS breadboard.**

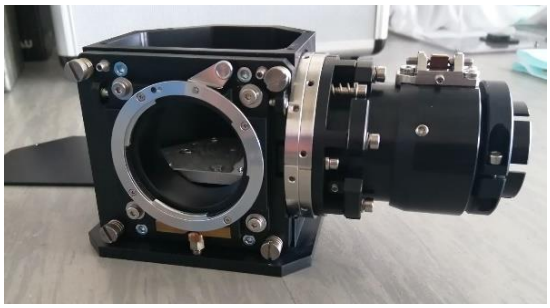

**Figure 3-9: SHS housing with lens interfaces.**

## 4. TEST AND CHARACTERIZATION CAPABILITIES

To test and characterize the SHS, extensive setups were developed that allow the characterisation of the imaging system and of the spectroscopic aspects of the instrument. A non-monolithic SHS breadboard has been built within a research work [9] to develop the test setup that it can be used for the MiniSPEC breadboard.

### 4.1. Characterization of the Imaging System

The MTF of both the fore-optics and detector optics have been measured through the slanted edge measurement method and through interferometric measurement using a six inch Zygo interferometer. The independent measurement allows to verify the measurement process and to utilize the advantages of the measurement principles, which are high precision for the interferometric measurement and fast full-field measurement for the slanted edge method. Figure 4-1 shows exemplarily the interferometric measurement setup of the detector optics wavefront measurement for MTF calculation.

The field of view and focal length is characterized with a focusable autocollimator on a tip-tilt stage that allows to measure at the relevant wavelength range of the instrument. The field of view can be directly measured up to 50 arcminutes. For larger values, it needs to be extrapolated based on the calculated focal length. The focal length was measured to 294.1 +/- 5.3 mm. The light source for the measurement is a red LED that covers the spectral bandwidth of the instrument. It can be used, because the focus of the autocollimator can be adjusted to use a different wavelength range then the nominal one in the green wavelength range.

All other tests use a monochromatic light source to characterize the system in dependence of wavelength. The light source is realized with a tuneable laser having a narrow line width (< 10 pm) and a scan range over the complete bandwidth of the filter. The tuneable laser is connected to a wavemeter for precise control of the wavelength (uncertainty: < 1 pm) and to a powermeter for controlling the light intensity (uncertainty < 1%) via a closed loop software controller. Using custom-made automation, it is possible to scan through the complete wavelength range of the SHS while recording wavelength, power, and SHS images. Figure 4-3 shows a picture of the monochromatic light source.

The monochromatic light source is used together with a telescope to provide a collimated source for transmission measurement of individual field points. The field position is first determined by the detector. Afterwards, the detector is removed and replaced by an integrating sphere to measure the transmitted power, relative to a previous power measurement without the instrument. The transmission of the overall system was calculated to >12% within the relevant wavelength range.

The point image on the detector of the collimated beam allows also to analyse ghosts in the system and is an approximation of the instrument PSF (if the telescope PSF is not corrected for).

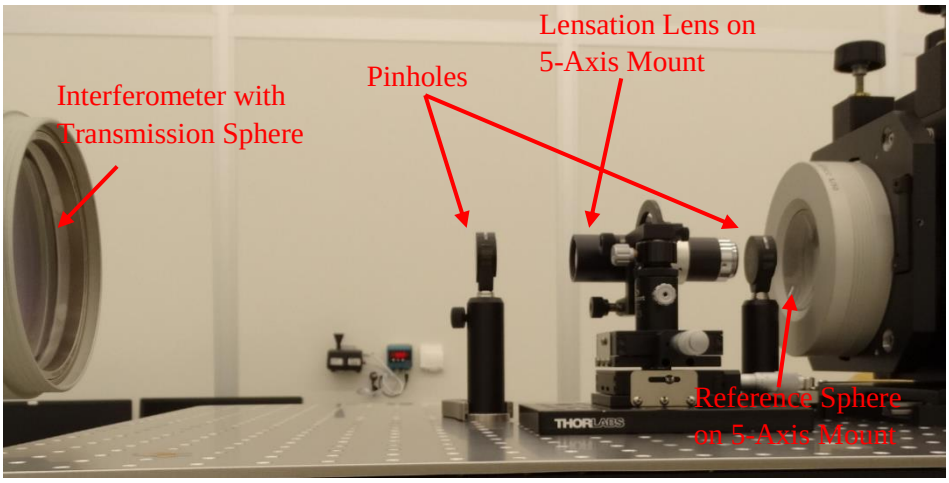


**Figure 4-1: Interferometric measurement setup for the wavefront of the detector optics lens.**

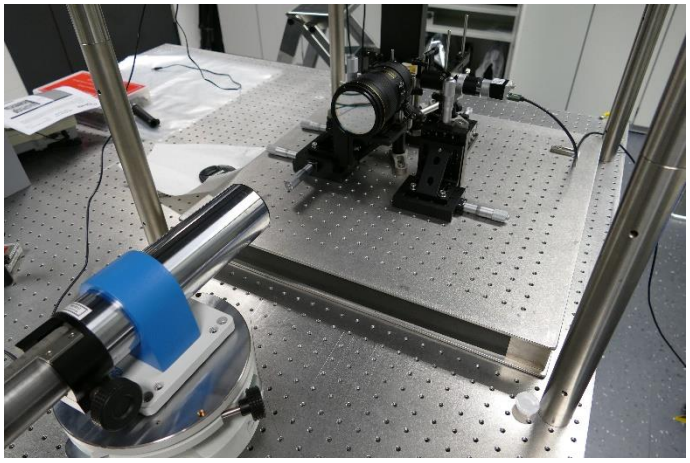

**Figure 4-2: Setup for distortion, field of view, and focal length measurement.**

### 4.2. Characterization of the Spectroscopy

For spectroscopic measurements, the light from the tuneable laser is injected into an integration sphere for uniform illumination of the complete aperture of the instrument, see Figure 4-4. Between fibre injection and integrating sphere, a speckle reducer minimizes the influence of speckle noise on the interferogram. A powermeter, coupled to the integration sphere, is used for power stabilization. A stability better than 0.25% (1-sigma) could be reached.

In addition to the tuneable laser illumination, a broadband source is mounted on the sphere. It is a red LED with a centre wavelength of 780 nm and a FWHM bandwidth of 22 nm that acts as white light source for the small spectral range of the instrument. The setup is readily extendable to other wavelength ranges by replacing the LED and the tuneable laser for the desired wavelength range.

This setup allows to perform a spectral line scan to calculate the spectrum in dependence of spatial frequency and wavelength. The relation between spatial frequency and wavelength is defined by the Littrow wavelength and the spectral conversion factor. The effective Littrow wavelength can be measured in this setup with an uncertainty better of +/- 1 pm, which allowed to characterize the SHS Littrow wavelength to 762.004 nm +/- 0.001 nm.

Additionally, the visibility of the interferograms can be computed for the complete image and in dependence of wavelength. The visibility ranges from 84% to 88% compared to the analytically calculated visibility of 88% to 95%. This information is then also used to calculate the spectral response of the instrument and to characterize the effective bandpass filter function. The spectral response measurement has currently an uncertainty of +/- 0.25% (1-sigma). Finally, the measured resolving power is 11788 +/- 35 for the SHS, compared to 12100 for the simulation with negligible wavelength dependence.

Temperature stability was tested in a thermal chamber in the range from -10°C to 50°C during a 12 h thermal cycle. The temperature stability was evaluated to -0.0933 +/- 0005 $cm^{-1}$/°C, which corresponds within < 20% to the analytic prediction.

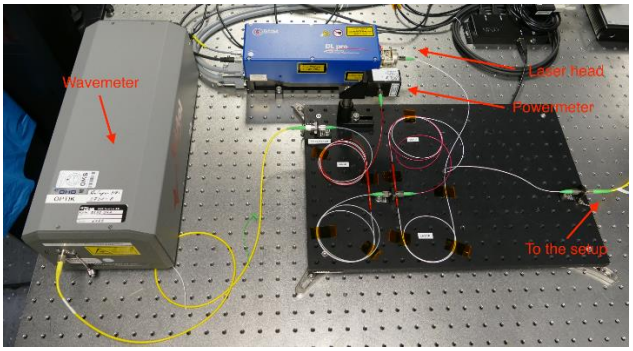


Figure 4-3: Characterisation setup: light source

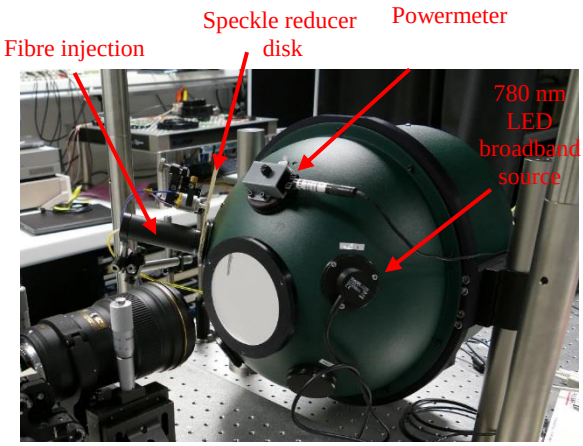


Figure 4-4: Characterisation setup: illumination

### 4.3. Correction of Instrument Artefacts

The data acquired with the tests above allow to correct for instrument artefacts. Specifically, three different corrections are being performed in the post-processing. The flatfield correction from Englert [10] is used to compensate for differences in arm transmission and pixel to pixel variation of the interferogram. The phase correction approach, described in [11], is used to correct for spatial frequency variations along the interferogram that result from image distortion. A relative radiometric calibration is performed afterwards to correct for the visibility decrease towards the edges of the image and for bandpass filter transmission variations.

## 5. DISCUSSION AND FURTHER DEVELOPMENT

### 5.1. MiniSPEC breadboard and test/characterisation setup

OHB together with MEOPTA gained through this project and previous experience with such types of instruments valuable knowhow that allowed the development of optics and optomechanics of SHS instruments. It includes the instrument requirement specification based on mission parameters, the design for an athermal and monolithic SHS that can be analysed with an extensive tool suite tailored for SHS optical systems. Thorough and tight interaction loops between design and manufacturing disciplines allow to design for manufacturing, assembly, and alignment. The ultra-high precision manufacturing capabilities facilitate the controlled and reproducible alignment of SHS, rendering batch and small series production feasible.

SHS can be characterized using state of the art, calibrated, and highly precise metrology setups for spectral, radiometric, geometric calibration and correction of instrument artefacts.

The overall in-depth understanding of the SHS technology allows the development of innovative design solutions for highly compact instruments with a high spectral resolution over a small bandwidth. Such systems may be ideal for Earth observation applications focusing on spectral bands of specific molecules/atoms, like the measurement of the oxygen A-band emission lines.

### 5.2. Towards a Satellite Instrument

The project developed a breadboard with focus on the monolithic SHS. The design of the SHS already considered special aspects of a satellite instrument, like temperature stability, ruggedness, outgassing and use of space qualified components. On the contrary, the fore-optics, detector optics, and SHS

housing interfaces were not chosen and designed based on utility in space missions. Thus, the next step towards a satellite instrument includes the development of these components. The engineering challenge lies there in the miniaturisation of the system and straylight suppression. Straylight suppression is an important topic for a limb viewing instrument and the development of fore-optics and detector optics needs to also consider a thorough treatment of this topic.

Hence, OHB together with Meopta started in 2022 with a follow-on project, in which the mission is further consolidated and the instrument is matured with the goal of an engineering model at the end of the project as preparation for a mission implementation phase.

## 6. ACKNOWLEDGEMENT

This breadboard development was conducted under the ESA EXPRO+ program 4000127312/19/NL/AR. We thank Christian Schwarz, Helene Strese, and Luca Maresi from ESA for their continued support, valuable feedback in reviews, and overall fruitful project work.

## 7. REFERENCES

[1] Connes, P., *Spectromètre Interférentiel à Sélection Par l'amplitude de Modulation*, J. phys. radium, 19, 215–222, 1958.

[2] Harlander, J. M., Reynolds, R. J., and Roesler, F. L., *Spatial Heterodyne Spectroscopy for the Exploration of Diffuse Interstellar Emission Lines at Far-Ultraviolet Wavelengths*, The Astrophysical Journal, 396, 730, 1992.

[3] Harlander, J. M., Roesler, F. L., Cardon, J. G., Englert, C. R., and Conway, R. R., *Shimmer: A Spatial Heterodyne Spectrometer for Remote Sensing of Earth' Middle Atmosphere*, Applied Optics, 41, 1343, 2002.

[4] Bourassa A.E., Langille, J., Solheim, B., Lloyd, N., Degenstein, D., Dupont, F., *The Spatial Heterodyne Observations of Water (SHOW) Instrument for High Resolution Profil in in the Upper Troposphere and Lower Statosphere*, Light, Energy and the Environment Congress, OSA, 2016.

[5] Deiml, M. and the AtmoHIT Team, *Test of a Remote Sensing Michelson-Interferometer for Temperature Measurements in the Mesosphere on a REXUS Rocket*, 23rd ESA PAC Symposium, Visby, Sweden, 2017

[6] Englert, C. R., et. al., *Michelson Interferometer for Global High-Resolution Thermospheric Imaging (MIGHTI): Instrument Design and Calibration*, Space Sci. Ref, 2017

[7] Mantel, K., Wroblowski, O., Olschweski, F., Kaufmann, M., *Spatial Heterodyne Interferometer for Temperature Measurements in the MLT Region of the Atmosphere*, ESA Workshop for Innovative Technologies for Space Optics, 2019

[8] Deiml, M., *Development of a Small Satellite Remote Sensing Payload for Passive Limb Sounding of the Atmospheric Oxygen Emission*, PhD Thesis, University of Wuppertal, 2017

[9] Robles, P. R., *Verification and Calibration of a Static Imaging Fourier-Transform Spectrometer*, Masterthesis, Technische Universität München, 2020

[10] Englert; C. R. Harlander; J. M., *Flatfielding in spatial heterodyne spectroscopy*, Applied Optics, vol. 45, no. 19; 2006.

[11] Englert, C. R., Harlander, J. M., Cardon, J. G., Roesler, F. L., *Correction of phase distortion in spatial heterodyne spectroscopy*, Applied Optics, vol. 43, no. 36, 2004.